06

Experimental determination of residual strains and stresses in 2G HTS wire

© A.V. Irodova, I.D. Karpov, O.A. Kondratiev, V.S. Kruglov, V.E. Krylov, S.V. Shavkin, V.T. Em

National Research Center „Kurchatov Institute“,
123182 Moscow, Russia
e-mail: Irodova_AV@nrcki.ru

Received May 18, 2024
Revised November 22, 2024
Accepted November 29, 2024

Using X-ray and neutron diffraction, residual strains and stresses were measured in the main components of the second generation high temperature superconducting (2G HTS) wire based on yttrium ceramics, which was produced at the National Research Center „Kurchatov Institute“ — in the stainless steel carrier tape, $Y_{0.15}Zr_{0.85}O_2$ and CeO_2 buffer layers, and the $YBa_2Cu_3O_7$ superconducting layer. Their changes during the wire manufacturing process were traced. The reliability of the results obtained is confirmed by their consistency. The method presented in the work for determining internal strain and stress is universal and is suitable for wires with different carrier tapes, buffer and superconducting layers.

Keywords: 2G HTS, residual strain/stress, AISI 310S tape, YSZ, CeO_2, YBCO, X-ray diffraction, neutron diffraction.

DOI: 10.61011/TP.2025.04.61210.185-24

Introduction

Second generation superconducting tape-wires based on the high-temperature superconductors $RBa_2Cu_3O_{7-\delta}$, where R — yttrium (YBCO) or rare-earth metal (REBCO), hereinafter referred to as 2G HTS are used today for manufacturing current-carrying elements of high-current cables designed to create plants with magnetic fields up to 20 T. They have a multilayer structure [1] with three main components:

1 — steel carrier tape-substrate with a thickness of several tens of microns which provides mechanical strength of the wire;

2 — single-crystal superconducting YBCO or REBCO layer with a thickness of about one micron which determines the conductive characteristics of the wire;

3 — buffer layers with a biaxial texture with a thickness from several microns to tenths of a micron which connect the superconducting layer with the carrier tape.

Other components of the wire perform protective and stabilizing functions.

When operating in strong magnetic fields, 2GHTS must withstand high tensile stresses without loss of current-carrying capacity. As a result of systematic tensile tests of wires with different carrier tapes, buffer and superconducting layers at temperatures from 4.2 to 300 K it was established that the electromechanical stability of the wire is ensured not only by the carrier tape but also by internal (residual) strains and stresses in the superconducting and buffer layers. Thus, the internal strain in the buffer layers affects the current-carrying capacity of the wire [2]. Internal strain in the superconducting layer prevents its destruction [3–7], which is also evidenced by the increased electromechanical stability of wires with a thin superconducting layer [8]. In addition to internal strain, the electromechanical properties of the wire are affected by the elastic domain microstructure in the superconducting layer [8–11], which changes under external load [12,13]. It is natural to think that it determines the internal strain in the superconducting layer.

Despite the importance of residual strains for 2GHTS, direct information about them is extremely limited and obtained indirectly through mechanical tests, and only for the superconducting layer [4–7]. As for residual stresses, just nothing is known about them. In order to get a complete representation about the residual strains and stresses, it is necessary to directly measure them in all components of the wire, which would seem unrealistic.

Previously, [14–16], we have developed and tested procedures which allow us to experimentally determine residual stresses and strains in separate components of 2GHTS.

Here we present the results obtained for the finished 2GHTS produced on the experimental technological line in the National Research Center „Kurchatov Institute“.

1. Methodology

1.1. Sample

The YBCO-based 2GHTS sample looked like this. A carrier tape was made of AISI 310S stainless steel. After several cycles of its polishing, a basic buffer layer of yttrium-stabilized zirconium dioxide $Y_{0.15}Zr_{0.85}O_2$ (YSZ) was applied to one of its side using the ABAD technique

Table 1. The main stages of 2GHTS manufacturing and the characteristics of the samples studied in the process

Sample	Designation	Manufacturing stage and sample characteristics	Ref. Research ref.
Initial tape AISI 310S	–	As supplied, cold-rolled semi-work-hardened. Thickness 100 μm, width 4 mm	[14–16]
Polished tape AISI 310S	#32	Several cycles of polishing by water suspension Al_2O_3 1–0.3 μm at the room temperature. Thickness about 98 μm	[15,16]
Tape with the basic buffer YSZ layer	YSZ#32	#32 + (layer of YSZ, ABAD 50 °C/36 h, the thickness 2.1 μm)	[15,16]
2GHTS	HTSC#272	YSZ#32 + (layer of CeO_2, PLD 700 °C/1 h, thickness 0.25 μm) + (layer of YBCO, PLD 750 °C/2 h, thickness 1.3 μm) + (layer of Ag, thermal sputtering, 100–150 °C, thickness 1.5 μm)+ annealing in oxygen 420 °C/2 h	Present work

(Alternating Beam Assisted Deposition). An additional buffer layer of CeO_2 and a subsequent superconducting layer of YBCO were applied to YSZ using the PLD method (Pulse Laser Deposition). The superconducting layer was protected by a layer of silver applied by thermal sputtering. After that the finished wire was annealed in an oxygen atmosphere. The main stages of wire manufacturing and the characteristics of the samples studied in the process are shown in Table 1.

1.2. Procedures

The methods for determining residual strains and stresses in 2GHTS components are described in detail in [14,16]. Let us briefly note the main points necessary for understanding the presented results.

• Residual stresses in thin layers, which are the buffer and superconducting layers of the wire, are determined using X-ray diffraction by strain they cause — the change in the distances d between the crystalline planes (hkl)[16].

• In single-crystal layers, strain and stress depend on the elastic constants of the crystal — the stiffness constants c_{ij} and the associated compliance constants s_{ij}. The elastic constants are specified in the unit cell of the crystal (the crystal coordinate system), the indices i, $j = 1, 2, 3$ correspond to its axes a, b, c.

• For layers with a cubic unit cell and a (001) interface with the substrate, as in YSZ and CeO_2, the strain and stress are isotropic. For any direction in the plane of the layer

$$\varepsilon_\psi = \frac{d_\psi - d_0}{d_0} = \sigma[2s_{12} + (s_{11} - s_{12})\sin^2\psi], \qquad (1)$$

where ε_ψ and σ — the relative strain and average stress in the layer, d_0 and d_ψ — the interplanar distances in the unstressed and stressed layer, ψ — the angle between the normal to the layer plane and the scattering vector perpendicular to the reflecting crystal plane.

• For a superconducting YBCO layer with an orthorhombic unit cell and a (001) interface with the substrate, the strain and stress are anisotropic [17]:

$$\varepsilon_\psi = A_1\sigma_{11} + A_2\sigma_{22}, \qquad (2)$$

$$A_1 = -\frac{\nu_{13}}{E_1} + \frac{1}{E_1}[(1+\nu_{12})\cos^2\xi + (\nu_{13} - \nu_{12})]\sin^2\psi,$$

$$A_2 = -\frac{\nu_{23}}{E_2} + \frac{1}{E_2}[(1+\nu_{21})\sin^2\xi + (\nu_{23} - \nu_{21})]\sin^2\psi,$$

$$E_1 = \frac{c_{11}c_{22}c_{33} + 2c_{23}c_{12}c_{13} - c_{11}c_{23}^2 - c_{22}c_{13}^2 - c_{33}c_{12}^2}{c_{22}c_{33} - c_{23}^2},$$

$$E_1 = \frac{c_{11}c_{22}c_{33} + 2c_{23}c_{12}c_{13} - c_{11}c_{23}^2 - c_{22}c_{13}^2 - c_{33}c_{12}^2}{c_{11}c_{33} - c_{13}^2},$$

$$\nu_{12} = \frac{c_{12}c_{33} - c_{13}c_{23}}{c_{22}c_{33} - c_{23}^2},$$

$$\nu_{21} = \frac{c_{12}c_{33} - c_{13}c_{23}}{c_{11}c_{33} - c_{13}^2},$$

$$\nu_{13} = \frac{c_{22}c_{13} - c_{12}c_{23}}{c_{22}c_{33} - c_{23}^2},$$

$$\nu_{23} = \frac{c_{11}c_{23} - c_{12}c_{13}}{c_{11}c_{33} - c_{13}^2},$$

where σ_{11} and σ_{22} — the stresses along the a and b axes of the orthorhombic cell, ξ — the angle between the direction in the layer and the a axis of the cell, E_i and ν_{ij} — the generalized Young's moduli and Poisson's ratios [18], the indices i, $j = 1, 2, 3$ correspond to the axes a, b, c of the orthorhombic cell.

In our case (see Fig. 1, on the left and Section 1.3), the axis a is directed either along the wire (in A domains, $\xi = 0$) or across it (in B domains, $\xi = 90°$). The strain ε_ψ is measured along the wire. For A domains

$$\varepsilon_\psi^{(A)} = \text{const} + \left(\frac{1+\nu_{13}}{E_1}\sigma_{11} + \frac{\nu_{23} - \nu_{21}}{E_2}\sigma_{22}\right)\sin^2\psi, \qquad (3.1)$$

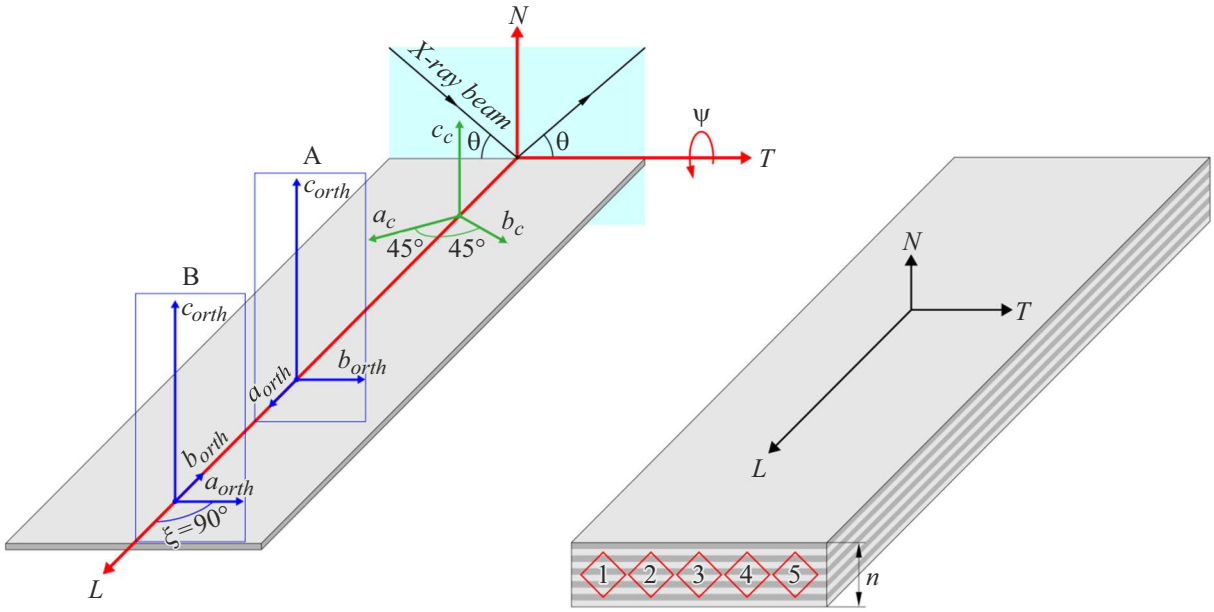

Figure 1. On the left — the setup of X-ray experiments and the used coordinate systems. L, T, N — laboratory coordinate system. a_c, b_c, c_c — crystal coordinate system for YSZ and CeO_2 buffer layers. a_{orth}, b_{orth}, c_{orth} — crystal coordinate system for YBCO superconducting layer, A ($\xi = 0°$) and B ($\xi = 90°$) domains. The mutual orientation of the laboratory and crystal systems is specified by the layer application technique. The residual strain in the layers was measured along L, on the planes of the crystal zones, the axes of which are parallel to T, the Bragg reflections from the planes were measured using the usual $\theta - 2\theta$ scheme in the scattering plane (T, N). On the right — the sample used in the neutron diffraction experiment: a packet of $n = 11$ wire segments. The arrows show the directions along (L), across (T) the rolling of the carrier tape and along the normal (N) to its plane (they coincide with the laboratory coordinate system). The probe volumes (points) in which the measurements were taken are numbered; their sections are shown in the plane (T, N), the sections in the plane (L, N) are the same. Details in the text.

for B domains

$$\varepsilon_\psi^{(B)} = \text{const} + \left(\frac{\nu_{13} - \nu_{12}}{E_1}\sigma_{11} + \frac{1 + \nu_{23}}{E_2}\sigma_{22}\right)\sin^2\psi, \tag{3.2}$$

where $\text{const} = -\left(\frac{\nu_{13}}{E_1}\sigma_{11} + \frac{\nu_{23}}{E_2}\sigma_{22}\right)$.

When we have measured $\varepsilon_\psi^{(A)}$ and $\varepsilon_\psi^{(B)}$, using the coefficients at $\sin^2\psi$ in (3.1) and (3.2) we can calculate σ_{11} and σ_{22}.

• In single-crystal layers, the strain ε_ψ is determined by the CGM (Crystallite Group Method) using crystal planes from different groups $\{hkl\}$, for details see [16]. If the conditions of the problem allow, it is convenient to use the planes of one crystal zone which includes a crystal plane parallel to the layer surface. The sample is rotated around the zone axis by angles ψ corresponding to the angles between the planes of the zone, and the interplanar distances are successively measured $d_\psi = d_{hkl}$.

• The residual strain ε_ψ is measured directly. The residual stress σ can be determined only if the elastic constants of the crystal are known. The elastic constants used in the present work are given in Tables 2.1 and 2.2. For YSZ the values are taken from [16], for CeO_2 they are determined similarly to [16] by data from [19–24], for YBCO they are calculated using formulas (2) and data from [25].

• The residual strain in the carrier tape of the wire $\varepsilon = (d - d_0)/d_0$ (where d_0 and d — the interplanar distances in the unstressed and stressed tape) is measured using neutron diffraction [14,15]. Suitable reflections hkl are used for the measurements. At each point of the sample, three strain components are measured: ε_L, ε_T and ε_N — along (L), across (T) the rolling and along normal (N) to the tape plane. Then they are taken to calculate the stress components

$$\sigma_i = E\,\frac{(1 - 2\nu)\varepsilon_i + \nu(\varepsilon_T + \varepsilon_N + \varepsilon_L)}{(1 + \nu)(1 - 2\nu)}, \tag{4}$$

where E — Young's modulus, ν — Poisson's ratio, $i = L, T, N$. For the AISI 310S stainless steel: $E = 200$ GPa, $\nu = 0.27$ [26], the measurements are carried out on reflections from the planes $\{311\}$.

• The reliability of determining the residual stresses in 2GHTS can be evaluated by the degree of consistency of the results obtained by different methods for different components of the wire [16].

1.3. X-ray measurements

The measurements were performed in the resource center of the laboratory X-ray methods „Roentgen" of the National

Table 2.1. Elastic stiffness constants c_{ij} and calculated compliance constants s_{ij} for cubic YSZ and CeO_2 single crystals

	c_{11}, GPa	c_{12}, GPa	s_{11}, GPa^{-1}	s_{12}, GPa^{-1}
YSZ	405.8(8.1)	95.5(13.9)	0.00271(7)	−0.00052(7)
CeO_2	390.9(42.1)	124.8(24.7)	0.00307(37)	−0.00074(14)

Note. For YSZ the values are taken from [16], for CeO_2 they are determined similarly to [16] using the original data [19–24]. The brackets contain standard deviations and errors in last characters.

Table 2.2. Elastic stiffness constants c_{ij} for an orthorhombic YBCO single crystal (error for c_{33} 7 %, in other cases 0.3 %) [25] and the generalized Young's moduli E_i and Poisson's ratios ν_{ij} calculated by the formulas (2)

	c_{11}, GPa	c_{22}, GPa	c_{33}, GPa	c_{12}, GPa	c_{13}, GPa	c_{23}, GPa
YBCO	231	268	186	132	71	95
	E_1, GPa	E_2, GPa	ν_{21}	ν_{12}	ν_{23}	ν_{13}
	162.1	174.5	0.470	0.436	0.332	0.159

Research Center „Kurchatov Institute“ [27] on the four-circle diffractometer Rigaku SmartLab using CuK_α-radiation and a beam with a point focus of 100 μm diameter at the room temperature. General details of sample preparation, the measurements and processing of the data obtained are given in [16]. The experimental setup is shown in Fig. 1, on the left.

The measurements were carried out in the laboratory coordinate system L, T, N, as defined by the wire geometry. The L and T axes are in the plane of the wire, along and across it, respectively, and the N axis is perpendicular to the wire plane.

The crystal coordinate systems, in which the elastic constants for YSZ, CeO_2 and YBCO are specified, are determined by the crystal symmetry. The crystal system a_c, b_c, c_c corresponds to the cubic symmetry of YSZ and CeO_2 (CaF_2 structure type). The crystal system a_{orth}, b_{orth}, c_{orth} corresponds to the orthorhombic symmetry of YBCO. The mutual orientation of the laboratory and crystal systems is specified by the layer application technique. The cubic axes a_c and b_c are in the wire plane at angles of 45° to the axes L and T, the axis c_c is directed along N. The orthorhombic axes a_{orth} and b_{orth} are also in the wire plane and the axis c_{orth} is directed along N. There are two possible orientations of the axes a_{orth} and b_{orth} relative to L and T, which differ in their rotation around the axis N by an angle of $\xi = 90°$:

(A) — a_{orth} along L, b_{orth} along T;

(B) — a_{orth} along T, b_{orth} along L.

They correspond to domains A and B formed by microtwins in the YBCO crystal [10,11,28].

The strain ε_ψ was measured on the planes of the crystalline zones with axes directed along T, and the planes with the most strong reflections were selected. For the isostructural YSZ and CeO_2, these are the (002), (11$\bar{3}$), (111), (331) planes which belong to the zone with the [1$\bar{1}$0] axis. For YBCO — the (001), (108), (103), (303) planes of the [010] zone for the domains A, and the (001), (018), (013), (033) planes of the [100] zone for the domains B. The transition from one crystal plane to another was performed by rotating the sample around the T axis by the respective angle ψ. The Bragg reflections were measured using the usual $\theta - 2\theta$ scheme in the scattering plane (T, N) (marked in turquoise in Fig. 1).

Since the protective silver layer strongly absorbs CuK_α-radiation and weakens the intensities of reflections in several times (Fig. 2), it was removed by etching the sample in the aqueous solution H_2O_2 30 % (1 volume part) + NH_4OH 3 % (3 volume parts). According to X-ray and electron microscopic data, such etching did not affect the YSZ, CeO_2 and YBCO layers in any way.

1.4. Neutron measurements

The measurements were carried out at the neutron stress diffractometry station STRESS [29] of the Kurchatov Neutron Research Complex IR-8 [30]. Sample preparation and measurement procedure are described in detail in [14,15]. The sample was a package of eleven wire segments of the same length of 50 mm (Fig. 1, on the right) which were cut from a single piece of the wire and successively laid on each other while maintaining the orientation relative to the wire side and the rolling direction of the carrier tape; the package was fixed in the aluminum case. Measurements were carried out through a layer of aluminum in five points (probe volumes) along the width of the wire, which were located in the middle of the length and thickness of the sample (the numbered points in Fig. 1). The single-crystal layers of YSZ, CeO_2 and YBCO in the wire, the total thickness of which is less than 4 % of the wire thickness, are invisible for neutrons, so the strain inside the carrier tape was actually measured. As in the case of the tape with

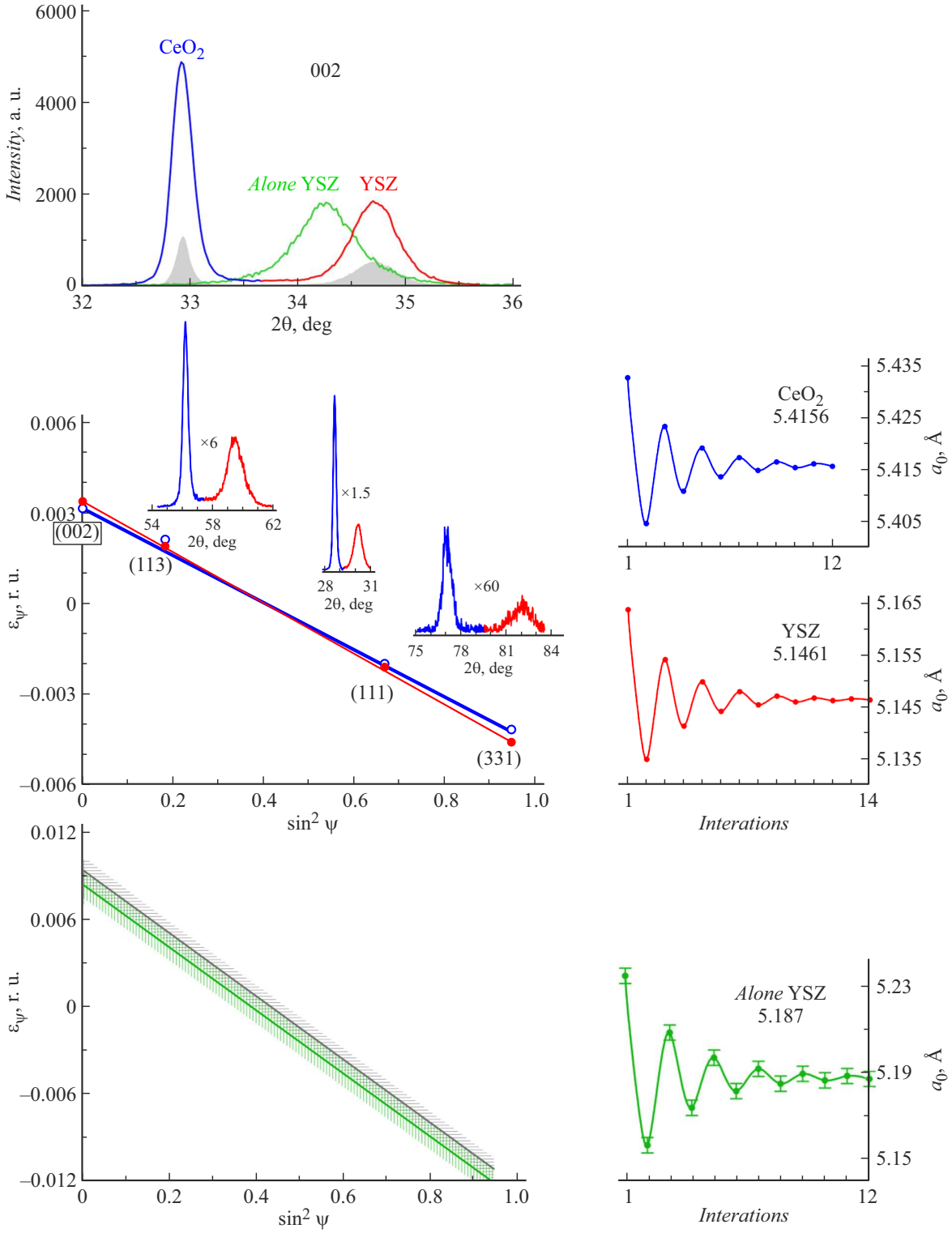

Figure 2. Results of X-ray measurements for YSZ (red) and CeO_2 (blue) layers in 2GHTS, CuK_α-radiation. For comparison, similar data for a single YSZ layer [16] are shown in green. At the top — Bragg reflections 002 in the sample without protective silver layer; reflections taken through a silver layer of 1.5 μm are shown in grey. In the center — relative strain ε_ψ for planes (002), (113), (111), (331) of the $[1\bar{1}0]$crystal zone; symbols — experimental points, errors within the symbols; lines — approximating straights $\varepsilon_\psi = k_0 + k_1 \sin^2 \psi$, standard deviations within the line thicknesses. For each plane, profiles of Bragg reflections are shown (for the (002) planes — at the top); the scale on the intensity axis is the same in all cases (as for 002). The iterative dependences for determining the periods a_0 for unstressed lattices are shown on the right. At the bottom — the data for a single YSZ layer [16], which correspond to the period a_0 determined by the iterative method. Within the standard deviation (shaded area), they coincide with those determined in [16] (shown in grey). Details in the text.

Table 3. Residual strain and stress in the buffer and superconducting layers of 2GHTS

Layer	Parameters of unstressed unit cell, Å			Domains	Strain, rel. un. $\varepsilon_\psi = k_0 + k_1 \sin^2\psi$		Stress, GPa
	a_0	b_0	c_0		k_0	k_1	
YSZ	5.1461(3)	–	–	–	0.0034(1)	−0.0084(2)	−2.60(16)
CeO_2	5.4156(6)	–	–	–	0.0032(2)	−0.0080(4)	−2.09(38)
YBCO	3.8162(6)	3.8839(6)	11.668(2)	A	0.0073(2)	−0.0101(4)	Along the wire, σ_{11} −1.63(16) Across the wire, σ_{22} −1.98(19)
				B	0.0073(3)	−0.0123(6)	Along the wire, σ_{22} −1.98(19) Across the wire, σ_{11} −1.63(16)
				30 %A + 70 %B	–	–	Along the wire −1.88(18) Across the wire −1.74(17)

Note: The strain is represented as the linear function $\varepsilon_\psi = k_0 + k_1 \sin^2\psi$ (Fig. 2, 3). The stress is calculated by the coefficient k_1 using the formulas (1), (3.1), (3.2) and the elastic constants of Tables 2.1 and 2.2. The brackets contain errors in last characters.

a single YSZ layer [15], the sample thickness was increased by an additional segment compared to the initial tape [14] because the wire is bent towards the single-crystal layers and there is a risk of output of the probe volume beyond the sample limits, especially during transverse (T) and normal (N) strain measurements when an increased-by-height probe volume is used [14].

2. Results

2.1. YSZ and CeO_2 layers

The experimental data for YSZ and CeO_2 layers are shown in Fig. 2. The main problem in determining the strain ε_ψ by the formula (1) is knowledge of the interplanar spacings d_0 or, for a cubic lattice, the period a_0 in the unstressed state. Unlike the tape with a single YSZ layer [15], in the finished wire it is impossible to experimentally produce unstressed states for the YSZ and CeO_2 layers. Therefore, for determination of a_0 we used the following iterative method.

The isotropic strain ε_ψ in the YSZ and CeO_2 layers can be represented as [31]:

$$\varepsilon_\psi = \varepsilon_\perp + (\varepsilon_\parallel - \varepsilon_\perp)\sin^2\psi,$$

where $\varepsilon_\parallel$ and $\varepsilon_\perp$ — the strain in the layer plane and perpendicular to it. Since $\varepsilon_\psi \le 1\%$ [16], the parameters of both the stressed and unstressed unit cell are close to $a_\perp = 2d_{002}$, where d_{002} — the measured distance between the (002) planes parallel to the layer surface ($\psi = 0$). We take $a_0 \approx a_\perp$.

1) Approximate the experimental points with a straight line $\varepsilon_\psi = k_0 + k_\perp \sin^2\psi$

2) Extrapolate the approximating line to $\psi = 90^\circ$ and obtain the strain in the layer plane $\varepsilon_\parallel = k_0 + k_1$.

3) Find the cell parameter in the layer plane $a_\parallel = a_0(\varepsilon_\parallel + 1) \approx a_\perp(\varepsilon_\parallel + 1)$

4) Determine a_0 for the next iteration: $a_0 = (a_\perp a_\parallel^2)^{1/3} \approx a_\perp(\varepsilon_\parallel + 1)^{2/3}$

Steps 1–4 are repeated until the difference in the values of a_0 for two consecutive iterations is equal to the accuracy of determining a_0 in them. The result is achieved in less than 15 iterations (Fig. 2, on the right).

The method was successfully tested on data for a single YSZ layer [16] (Fig. 2, at the bottom). The obtained value $a_0 = 5.187(4)$ Å is in satisfactory agreement with the experimental one, 5.182 Å, and the strain calculated with it coincides within the standard deviation with that determined in [16].

The results of processing the experimental data for the YSZ and CeO_2 layers are given in Table 3. The values of a_0 are somewhat higher than for conventional crystals — by 0.22 % and 0.085 %, respectively. It is not surprising, especially for the basic buffer layer of YSZ whose lattice is initially strongly swelled [16]. The residual strain in both layers is compressive. The compressive stress in CeO_2 is less than in YSZ by approximately 20 %. The stress in YSZ is less than in a single layer [16] also by 20 %.

2.2. YBCO layer

Experimental data for the YBCO layer are shown in Fig. 3.

Unlike YSZ and CeO_2, in YBCO the iteration method is not suitable for determining the parameters of the unstressed unit cell because there are three parameters: a_0, b_0 and c_0. Therefore, we applied a different approach using the ratio of these parameters for a conventional (unstressed) ceramics $YBa_2Cu_3O_{7-\delta}$ [32–37] and the fact that the cell volume is preserved during the transition from the stressed to the unstressed state (since the residual stresses are elastic). In conventional ceramics, $a_0 : b_0 : c_0 = 0.3271(5) : 0.3329(5) : 1$ [32–37] and, accordingly, the cell volume $V_0 = a_0 b_0 c_0 = 0.1089(3)c_0^3$. The

volume of the stressed cell in the YBCO layer determined from the experimental data is $V = 172.94(8)$ Å^3. Since it is preserved during the transition from the stressed to unstressed state, the absolute values of the parameters of the unstressed cell (Table 3) can be easily found from the equality $V = 172.94(8) = V_0 = a_0 b_0 c_0 = 0.1089(3) c_0^3$ and the ratio $a_0 : b_0 : c_0$; the difference with the usual parameters [32–37] is less than 0.05%. Other results of processing the experimental data for the YBCO layer are given in Table 3.

An interesting result is the predominance in the YBCO layer of B domains with the long axis of the unit cell directed along the wire (Fig. 1). As estimated from the ratio of Bragg intensities for domains A and B (Fig. 3), they constitute approximately 70%, domains A — 30%. The compressive stress along the wire in B domains is greater than in A domains by approximately 20%. The resulting compressive stress in the YBCO layer along the wire is −1.88 GPa, which is almost 8% greater than across it, −1.74 GPa. The average stress in the YBCO layer is 14% less than in the underlying CeO_2 layer. The predominance of B domains in the YBCO layer was explained by neutron measurements of the carrier tape.

2.3. Carrier tape AISI 310S

The results of determining the residual strains and stresses in the carrier tape of the wire are shown in Fig. 4.

Strikingly, there is a strong, almost 2.5-fold, increase in longitudinal strain ε_L compared to that in the tape with a single YSZ layer [15], while transverse ε_T and normal ε_N strains decreased proportionally. The longitudinal tensile stress $\sigma_L = 169(32)$ MPa also increased by 2.5 times, the transverse $\sigma_T = 68(23)$ MPa remained practically unchanged, the normal $\langle\sigma_N\rangle$ was taken to be equal to zero, as in [14,15]. The redistribution of strains and stresses across the width of the tape occurred within the standard deviations.

The observed picture cannot be explained in terms of the balance of elastic forces in the wire if we take into account the compressive stresses only in the buffer and superconducting layers (Table 3). In this case, the calculated tensile stress across the tape, 82(7) MPa, is close to the transverse stress σ_T, while the calculated stress along the tape, 84(7) MPa, is half the longitudinal σ_L (blue area in Fig. 4). The compressive stress on the tape surface under the YSZ layer, determined in the same way as in [16], also does not agree with the calculation. The calculated stress, −372(28) MPa, is less than that in the tape with a single YSZ layer, −720(53) MPa, but −331 MPa greater than that in the tape in the wire, −41(110) MPa, (Fig. 4, blue area in the inset at the bottom).

Thus, to maintain the balance of elastic forces, an additional tensile stress of $\Delta\sigma_L \approx 85$ MPa is required inside the tape and approximately four times greater on its surface, in agreement with [31]. It is easy to understand its origin

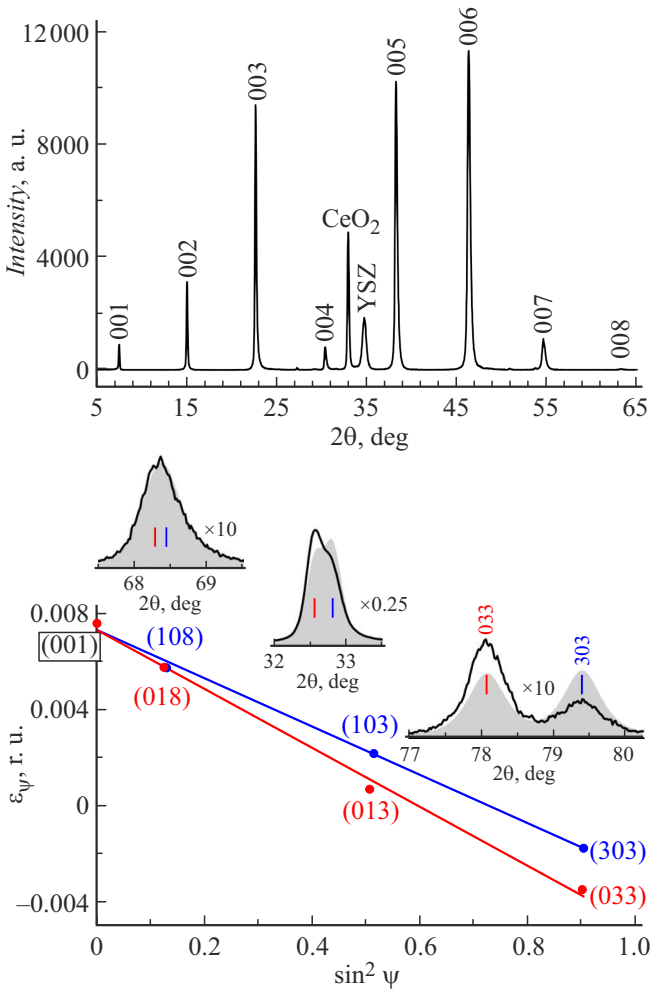

Figure 3. Results of X-ray measurements for the YBCO layer, CuK_α-radiation. At the top — general diffraction pattern for the wire without protective silver layer. Reflection indices from YBCO in the orthorhombic cell. At the bottom — relative strain ε_ψ for (001), (108), (103), (303) planes of the [010] crystalline zone in domains A (blue), and (001), (018), (013), (033) planes of the [100] zone in domains B (red), Fig. 1; for the (001) plane, averaging over strong 003, 005, 006 reflections was used. Symbols — experimental points, errors within the symbols; lines — approximating straight $\varepsilon_\psi = k_0 + k_1 \sin^2\psi$, standard deviations within the line thicknesses. In Bragg reflection profiles, vertical dashes show positions of reflections from A and B domains; the scale for intensity axis is the same in all cases (as in general pattern at the top). Reflections profiles calculated for the equally probable distribution of A and B domains in a $YBa_2Cu_3O_{7-\delta}$ single crystal, $0 \le \delta < 0.5$, are shown in grey.

(Table 1). The CeO_2 and YBCO layers are applied at a temperature of 700−750 °C for 3 h. To avoid sagging of the wire, it is stretched at this temperature and left in this state during subsequent application of the protective layer, annealing in oxygen and cooling to the room temperature. As a result, excess tensile stress occurs in the carrier tape. It is maximal on the surface of the tape and decreases with depth (Fig. 4, grey area in the insert at the bottom),

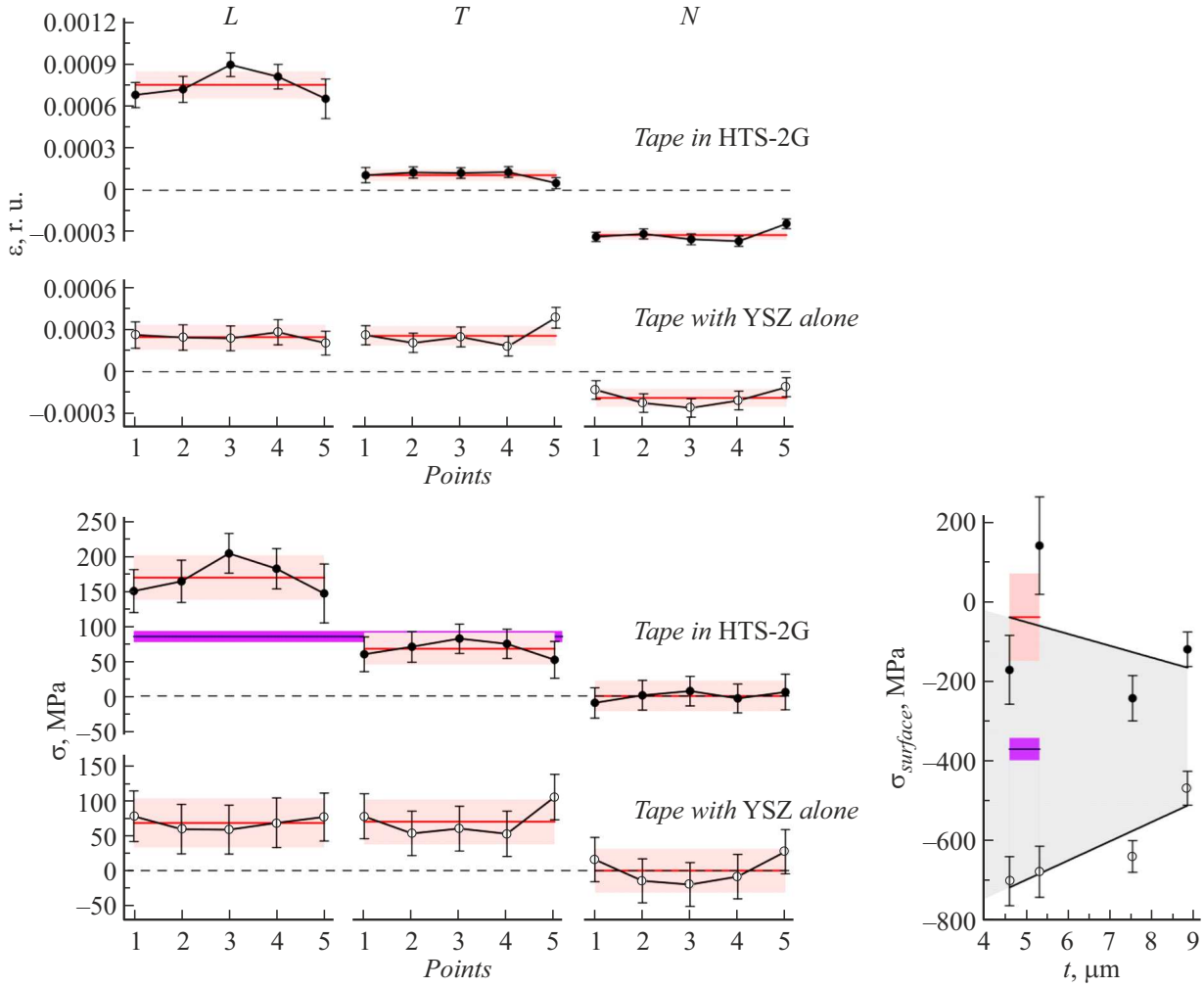

Figure 4. Residual strain ε and stress σ (L, T and N components, Fig. 1) in the carrier tape in 2GHTS, in comparison with the data for the tape with a single YSZ layer [15]. The positions of the probe volumes (*Points*) are shown in Fig. 1. Symbols (black circles for tape in wire, white circles for tape with a single YSZ layer) — experimental points with errors, connected by lines for eye; mean values and standard deviation areas are shown in red. The value of σ with error, calculated from the X-ray data from Table 3, is shown in blue. In the inset at the bottom right — the stress $\sigma_{surface}$ on tape surface under YSZ layer in the wire and in the tape with a single YSZ layer [16] depending on surface layer thickness t; symbols — experimental points with errors, gray area corresponds to tensile stress. The value of $\sigma_{surface}$ with error, determined from measured stress σ_L, is shown in red. The value of $\sigma_{surface}$ with error, calculated from X-ray data, is shown in blue. Details in the text.

while a compressed layer is preserved on the surface of the tape. According to the estimate, the balance of elastic forces is achieved when a compressed layer thickness is about $15\,\mu$m and an average stress in it is -360 MPa. A layer with such parameters is invisible to neutrons [15], and only the additional tensile stress $\Delta\sigma_L$ along the tape is observed.

The tension of the wire during the manufacturing process and subsequent annealing in this state naturally explain the predominance in the YBCO layer of B domains with higher compressive stress and a long axis of the unit cell along the wire. This is the result of minimization of elastic energy in the wire. Previously [12,13], a similar effect was observed in finished wires subjected to additional annealing under load.

Conclusion

The main results:

1. Residual strains and stresses in the main components of the finished 2GHTS are measured for the first time. The wire was manufactured at the National Research Center „Kurchatov Institute“.

2. In the YSZ and CeO_2 buffer layers and the YBCO superconducting layer, the strain and stress are compressive. The stress decreases from YSZ (-2.60 GPa) to CeO_2 (-2.09 GPa) and YBCO (-1.81 GPa in average), by 20 % and 14 %, respectively. In the superconducting layer, the domains with higher compressive stress and long axis of the unit cell along the wire predominate, they constitute 70 %.

3. In the AISI 310S carrier tape, the stress is tensile and highly anisotropic along (169 MPa) and across (68 MPa) the wire. Excessive longitudinal stretching is caused by conditions of wire manufacturing, which are responsible for predominance in the superconducting layer of domains with high compressive stress along the wire.

4. The reliability of the obtained results is confirmed by their consistency.

5. Simple methods for determining the parameters of unstressed state for 2GHTS main components, based on available data for stressed state, are proposed.

6. The method for determining internal strains and stresses in 2GHTS presented in the work is universal. It uses well-known proven procedures and is suitable for wires with different carrier tapes, buffer and superconducting layers.

Acknowledgments

The authors are grateful to I.V. Kulikov for assistance in etching the wire.

Funding

The work was carried out under state assignment of the National Research Center „Kurchatov Institute“.

Conflict of interest

The authors declare that they have no conflict of interest.

References

[1] J.L. MacManus-Driscoll, S.C. Wimbush. Nat. Rev. Mater., **6**, 587 (2021). DOI: 10.1038/s41578-021-00290-3

[2] M. Sugano, K. Osamura, W. Prusseit, R. Semerad, K. Itoh, T. Kiyoshi. Supercond. Sci. Technol., **18**, 369 (2005). DOI: 10.1088/0953-2048/18/3/027

[3] K. Osamura, M. Sugano, S. Machiya, H. Adachi, M. Sato, S. Ochiai, A. Otto. Supercond. Sci. Technol., **20**, S211 (2007). DOI: 10.1088/0953-2048/20/9/S15

[4] M. Sugano, S. Machiya, K. Osamura, H. Adachi, M. Sato, R. Semerad, W. Prusseit. Supercond. Sci. Technol., **22**, 015002 (2009). DOI: 10.1088/0953-2048/22/1/015002

[5] K. Osamura, M. Sugano, S. Machiya, H. Adachi, S. Ochiai, M. Sato. Supercond. Sci. Technol., **22**, 065001 (2009). DOI: 10.1088/0953-2048/22/6/065001

[6] K. Osamura, S. Machiya, Y. Tsuchiya, H. Suzuki. Supercond. Sci. Technol., **23**, 045020 (2010). DOI: 10.1088/0953-2048/23/4/045020

[7] K. Osamura, S. Machiya, Y. Tsuchiya, H. Suzuki. IEEE Trans. Appl. Supercond., **20** (3), 1532 (2010). DOI: 10.1109/TASC.2010.2042437

[8] A. Krivykh, A. Irodova, V. Krylov, I. Kulikov, A. Polyakov. IEEE Trans. Appl. Supercond., **32** (4), 8400105 (2022). DOI: 10.1109/TASC.2022.3143773

[9] K. Osamura, S. Machiya, Y. Tsuchiya, S. Harjo, H. Suzuki, T. Shobu, K. Kiriyama, M. Sugano. IEEE Trans. Appl. Supercond., **21** (3), 3090 (2011). DOI: 10.1109/TASC.2010.2086038

[10] K. Osamura, S. Machiya, Y. Tsuchiya, H. Suzuki, T. Shobu, M. Sato, S. Ochiai. IEEE Trans. Appl. Supercond., **22** (1), 8400809 (2012). DOI: 10.1109/TASC.2011.2178847

[11] K. Osamura, S. Machiya, D.P. Hampshire. Supercond. Sci. Technol., **29**, 065019 (2016). DOI: 10.1088/0953-2048/29/6/065019

[12] S. Awaji, T. Suzuki, H. Oguro, K. Watanabe, K. Matsumoto. Sci. Rep., **5**, 11156 (2015). DOI: 10.1038/srep11156

[13] T. Okada, H. Misaizu, S. Awaji. IEEE Trans. Appl. Supercond., **31** (5), 6601006 (2021). DOI: 10.1109/TASC.2021.3063995

[14] I.D. Karpov, A.V. Irodova, V.S. Kruglov, S.V. Shavkin, V.T. Em. Tech. Phys., **65** (7), 1051 (2020). DOI: 10.1134/S1063784220070063

[15] A.V. Irodova, I.D. Karpov, V.S. Kruglov, V.E. Krylov, S.V. Shavkin, V.T. Em. Tech. Phys., **67** (15), 2391 (2022). DOI: 10.21883/TP.2022.15.55265.169-21

[16] A.V. Irodova, E.A. Golovkova, O.A. Kondratiev, V.S. Kruglov, V.E. Krylov, S.A. Tikhomirov, S.V. Shavkin. Tech. Phys., **67** (12), 1603 (2022). DOI: 10.21883/TP.2022.12.55196.197-22

[17] E.M. Santos, M.T.D. Orlando, M.S.R. Miltao, L.G. Martinez, A.S. Alves, C.A. Passos. Jpn. J. Appl. Phys., **49**, 056601 (2010). DOI: 10.1143/JJAP.49.056601

[18] A.F. Bower. Applied Mechanics of Solids (CRC Press, Boca Raton, 2009), DOI: 10.1201/9781439802489

[19] W.H. Weber, K.C. Bass, J.R. McBride. Phys. Rev. B, **48**, 178 (1993). DOI: 10.1103/PhysRevB.48.178

[20] T. Gurel, R. Eryigit. Phys. Rev. B, **74**, 014302 (2006). DOI: 10.1103/PhysRevB.74.014302

[21] V. Kanchana, G. Vaitheeswaran, A. Svane, A. Delin. J. Phys.: Condens. Matter., **18**, 9615 (2006). DOI: 10.1088/0953-8984/18/42/008

[22] C. Sevik, T. Çagin. Phys. Rev. B, **80**, 014108 (2009). DOI: 10.1103/PhysRevB.80.014108

[23] J.C. Goldsby. J. Ceramics, **2013**, 323018 (2013). DOI: 10.1155/2013/323018

[24] K. Suzuki, M. Kato, T. Sunaoshi, H. Uno, U. Carvajal-Nunez, A.T. Nelson, K.J. McClellan. J. Am. Ceram. Soc., **102**, 1994 (2019). DOI: 10.1111/jace.16055

[25] Ming Lei, J.L. Sarrao, W.M. Visscher, T.M. Bell, J.D. Thompson, A. Migliori, U.W. Welp, B.W. Veal. Phys. Rev. B, **47**, 6154 (1993). DOI: 10.1103/PhysRevB.47.6154

[26] AISI 310S (S31008) Stainless Steel. [Electronic source] URL: https://www.makeitfrom.com/material-properties/AISI-310S-S31008-Stainless-Steel

[27] Resursny tsentr laboratornykh rentgenovskikh metodov „Rentgen“. (in Russian) URL: http://www.rc.nrcki.ru/pages/main/rentgen/index.shtml

[28] G.J. McIntyre, A. Renault, G. Collin. Phys. Rev. B, **37**, 5148 (1988). DOI: 10.1103/PhysRevB.37.5148

[29] V.T. Em, I.D. Karpov, V.A. Somenkov, V.P. Glazkov, A.M. Balagurov, V.V. Sumin, P. Mikula, J. Saroun. Physica B: Condens. Matter., **551**, 413 (2018). DOI: 10.1016/j.physb.2018.02.042

[30] Kurchatovkii neitronnyi issledovatel'skii kompleks IR-8. (in Russian) URL: http://kcsni.nrcki.ru/pages/main/IR8/beamlinesIR8/index.shtml

[31] L.B. Freund, S. Suresh. *Thin film materials. Stress, defect formation and surface evolution* (Cambridge University Press, NY., 2004), DOI: 10.1017/CBO9780511754715.003

[32] J.J. Capponi, C. Challout, A.W. Hewat, P. Lejay, M. Marezio, N. Nguyen, B. Raveau, J.L. Soubeyroux, J.L. Tholence, R. Tournier. Europhys. Lett., **3**, 1301 (1987). DOI: 10.1209/0295-5075/3/12/009
[33] R.J. Cava, B. Batlogg, C.H. Chen, E.A. Rietman, S.M. Zahurak, D. Werder. Phys. Rev. B, **36**, 5719 (1987). DOI: 10.1103/PhysRevB.36.5719
[34] R.J. Cava, B. Batlogg, R.B. van Dover, D.W. Murphy, S. Sunshine, T. Siegrist, J.P. Remeika, E.A. Rietman, S. Zahurak, G.P. Espinosa. Phys. Rev. Lett., **58**, 1676 (1987). DOI: 10.1103/PhysRevLett.58.1676
[35] W. David, W. Harrison, J. Gunn, O. Moze, A.K. Soper, P. Day, J.D. Jorgensen, D.G. Hinks, M.A. Beno, L. Soderholm, D.W. Capone, I.K. Schuller, C.U. Segre, K. Zhang, J.D. Grace. Nature, **327**, 310 (1987). DOI: 10.1038/327310a0
[36] O.K. Antson, P.E. Hiismaki, H.O. Poyry, A.T. Tiitta, K.M. Ullakko, V.A. Trunov, V.A. Ul'yanov. Solid State Comm., **64**, 757 (1987). DOI: 10.1016/0038-1098(87)90694-6
[37] H. You, R.K. McMullan, J.D. Axe, D.E. Cox, J.Z. Liu, G.W. Crabtree, D.J. Lam. Solid State Comm., **64**, 739 (1987). DOI: 10.1016/0038-1098(87)90690-9

Translated by M.Shevelev